Mine Water and the Environment (2021) 40:671–689
https://doi.org/10.1007/s10230-021-00791-1

TECHNICAL ARTICLE

Hydrogeological Analysis of Sulfide Tailings at a Uranium Mine Using Geophysical and Hydrochemical Methods

Débora Andrade Targa[1] · **César Augusto Moreira**[1] · **Matheus Felipe Stanfoca Casagrande**[1]

Received: 30 May 2020 / Accepted: 9 June 2021 / Published online: 15 June 2021
© Springer-Verlag GmbH Germany, part of Springer Nature 2021

Abstract

A hydrogeological analysis was conducted of aquifer systems within a sulfide-rich tailings pile and underlying rocks at a uranium mine to understand the generation and transport of AMD. A geophysical investigation was carried out along seven transects spaced 30 m apart using electrical resistivity tomography and a Wenner-Schlumberger array. The results were used as input to 2D and pseudo-3D models of resistivity and chargeability parameters. The geophysical results and models contrasted unaffected saturated zones and zones impacted by AMD, in addition to three areas within the tailings with a high sulfide content. The tailings and underlying fractured bedrock aquifer are hydrologically connected, which promotes the exchange of mine-influenced water into the regional aquifer. Releases from the site's tailings and other wastes can severely affect regional groundwater.

Keywords Acid mine drainage · Electrical resistivity tomography · Chargeability · Brazil

Introduction

The mining industry has experienced vigorous growth in recent decades due to profound socioeconomic changes around the world. When economic performance is high, investments in technology and effective solutions in environmental remediation of degraded areas is assumed from the earliest stages of mining. However, decommissioning and mine closure may be considered secondary priorities in mine planning because these activities add cost without financial return compared to mining and ore processing. This flawed argument can have disastrous consequences, such as recent tailings dam collapse at Brumadinho in Minas Gerais, Brazil (Rotta et al. 2020; Thompson et al. 2020).

Environmental management in mining activities has become a great societal concern due to growing awareness of tragedies that result from disregarding environmental protection (Armstrong et al. 2019; Glotov et al. 2018; Owen et al. 2020). Impositions from clients and investors for certifications and environmental recovery planning for mined areas have also contributed to improved legal compliance in this economic climate.

The Osamu Utsumi Mine, located at Caldas (State of Minas Gerais) in Brazil, has decommissioned a uranium mine to reduce environmental impacts and comply with current environmental regulations. One of the biggest challenges in this area is the volume of acid-generating waste material and tailings (Dutta et al. 2020; Freitas et al. 2011; Lei and Watkins 2005; Migaszewski et al. 2018; Moreno et al. 2020; Naicker et al. 2003; Yang et al. 2016).

Acid mine drainage (AMD) is produced as a consequence of chemical weathering of either a natural ore deposit or mining wastes. Consequently, the AMD can mix with groundwater flow and leach high concentrations of dissolved metals and other constituents from rocks and waste materials (Pabst et al. 2018; Simate and Ndlovu 2014). These effluents are especially enriched in metals that are mobile in oxidizing environments (Equeenuddin et al. 2013; Moyé et al. 2017; Nordstrom et al. 2015). In the case of a uranium mine, the mobilization of radioactive elements might contribute to the deterioration of the local water quality. Despite being a well understood process, AMD is extremely complex to

✉ Débora Andrade Targa
debora.targa@gmail.com

César Augusto Moreira
moreirac@rc.unesp.br

Matheus Felipe Stanfoca Casagrande
mfs-casagrande@hotmail.com

[1] Geosciences and Exact Sciences Institute (IGCE), São Paulo State University, 24-A Avenue, 1515, Bela Vista, Rio Claro, SP, Brazil

remediate and is often seen as an irreversible environmental liability with costly mitigation measures (Akcil and Koldas 2006).

Different depositional techniques and arrangements for waste rock and tailings can create a unique structural setting with specific hydraulic characteristics related to particle size and distribution and chemical composition that affect not only the underground flow patterns but also the heat and oxygen distribution (Anterrieu et al. 2010; Dawood and Aubertin 2014; Fala et al. 2003). Once built, the waste piles become part of the local hydrological system (Aubertin 2013). Thus, the wastes' hydrogeological, geotechnical, and chemical characteristics progressively change, exposing mineral assemblages to changing chemical equilibria. Sulfide minerals are a perfectly example because their oxidized ion (SO_4^{-2}) is highly mobile in groundwater.

Applied geophysics has been used to determine the characteristics of shallow structures for engineering site investigations, explore for groundwater and minerals and other economic resources, and to map buried cavities and archaeological remains. Geophysical methods have been increasingly used to investigate derelict and contaminated land and groundwater to locate contaminant plumes before digging pits and boreholes, including at sites affected by AMD from tailings (Epov et al. 2017; Martín-Crespo et al. 2018; Martínez-Pagán et al. 2021; Power et al. 2018; Targa et al. 2019).

Direct current (DC) resistivity and induced polarization (IP) methods are non-invasive, have great spatial coverage, and can be used to recognize inorganic contaminants in soils and rocks and to study the physical and geotechnical integrity of waste and tailings piles (Anterrieu et al. 2010; Casagrande et al. 2018, 2020; Spitzer and Chouteau 2003; Yuval and Oldenburg 1996). 2D and 3D geophysical modeling of the results from these geoelectrical methods combined with electrical resistivity tomography (ERT) can reliably and consistently identify the presence of acidic plumes and help determine their lateral and vertical extent (Bortnikova et al. 2018; Olenchenko et al. 2016).

We assessed underground flow of AMD within a tailings pile and its underlying rock at a uranium mine complex using DC resistivity and IP with 2D and pseudo-3D tomographic modeling. In addition, water quality data from groundwater samples were used to elucidate hydrogeological processes that could be occurring inside the tailings.

The Osamu Utsumi Mine

Geological and Hydrogeological Settings

The Osamu Utsumi Mine is part of an industrial mining complex of Poços de Caldas (CIPC) owned by Nuclear Industries of Brazil (INB-Indústrias Nucleares do Brasil), a government entity, and the location of the nation's first uranium production center. The CIPC is located in the southwest portion of Minas Gerais State, Brazil. It is part of the Poços de Caldas alkaline complex, which is a Mesozoic ring structure that comprises a suite of alkaline volcanic, subvolcanic, and plutonic rocks, mainly phonolites and nepheline syenites (Fig. 1) that is recognized worldwide as a naturally high radiation region (Veiga et al. 2003; Waber 1992). The mineral assemblages found in these rocks consists of K-feldspar, albite, Na-pyroxenes, nepheline, eudialyte, biotite, and sanidine, generally containing concentrations of U, Th, and rare earth elements.

Regional post-magmatic hydrothermal events promoted argillation and zeolitization of the rocks, and hydrothermal fluid-rocks interactions led to pyritization, strong potassium metasomatism, and formation of radioactive anomalies during the primary mineralizing event (Valeton et al. 1997; Waber et al. 1992). Typical mineralization includes pitchblende (U_3O_8), jordisite (MoS_2), sphalerite, zircon-baddeleyite (ZrO_2), fluorite, and pyrite (Schorscher and Shea 1992). The minerals are often disseminated without any evidence of structural control or association with fractured veins, stockwork systems, or local volcanic breccias (Cathles and Shea 1992). The final stage in the geological and mineralogic evolution of the Poços de Caldas alkaline complex involved the emplacement of carbonatite and mafic–ultramafic dyke rocks; weathering produced a lateritic weathered zone. Simultaneously, a downward-migrating oxidation front resulted in supergene remobilization and precipitation of uranium oxide as pitchblende and associated elements, which provided a secondary mineralizing event (Waber et al. 1992).

The uranium deposit of Poços de Caldas Plateau has an ore grade of 0.1% U, which is considered a poorly mineralized reserve. Uranium occurs as U(IV) and U(VI) oxides associated with pyrite (FeS_2), fluorite (CaF_2), and zirconium and molybdenum minerals. The discovery of promising caldasite deposits, a rare uriniferous ore of zircon ($ZrSiO_4$) and baddeleyite (ZrO_2), prompted the opening of the Osamu Utsumi Mine in 1959, in the southeast region of the alkaline complex (Cathles and Shea 1992; Schorscher and Osmond 1992) (see Fig. 1 for location).

The local geological context of the Osamu Utsumi Mine includes nepheline syenites and phonolites with stockwork mineralization superimposed on disseminated ore in volcanic breccias and fractured host rocks, which were subjected to hydrothermal alteration and metasomatic processes, resulting in potassic metasomatism and uranium mineralization. The volcanic suite of the Osamu Utsumi Mine has two main fracture systems at N20E/80NW and N55W/75NE, with orthogonal angles between them; their

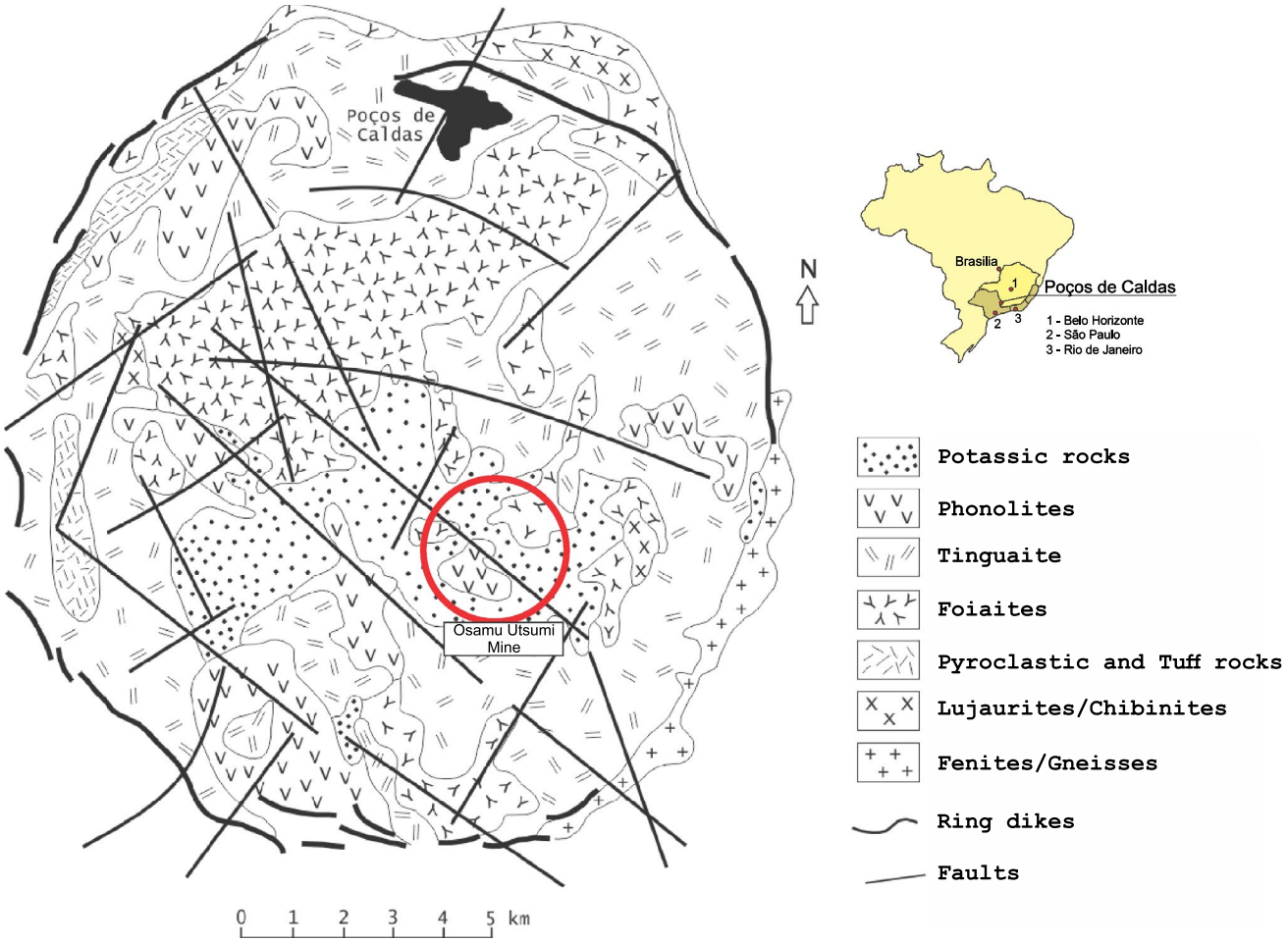

Fig. 1 Volcanic suite and geological structures of Alkaline Complex of Poços de Caldas showing Osamu Utsumi Mine locations (Modified of Fraenkel et al. 1985)

spatial arrangement promotes good hydraulic conductivity inside the rock mass (Targa et al. 2019).

The local hydrogeological setting is described as an unconfined porous aquifer in the weathered zone, which is hydraulically connected to the fractured nepheline syenite bedrock aquifer composed (Golder 2012). Meteoric water infiltrates the soil formed by bedrock weathering in the upper layers of the lithological sequence and is stored in its inherent porosity. Regional stress over the Poços de Caldas alkaline complex produced deep faults and fractures across the plateau, which allowed fresh water to infiltrate and percolate through the bedrock's secondary porosity.

Groundwater consists of a mixture of reducing groundwater, which flows through fractures in the bedrock, and oxidizing meteoric water. The local aquifer system is divided into three main zones: a shallow aquifer (B), an intermediate aquifer (C) that reaches up to 200 m deep, and a deep aquifer (D) that extends to around 2000 m deep (Costa et al. 1998; Cruz and Peixoto 1989). Table 1 indicates the main

Table 1 Physical–chemical parameters and ionic content of stream water (A), shallow zone (B), intermediate zone (C) and deep zone (D) of the local aquifer (Costa et al. 1998)

Parameter	A	B	C	D
Temperature (°C)	19.5	21.5	22.7	37.5
pH	6.6	6.00	7.5	9.8
Conductivity (μmho/cm)	25.7	49.8	110	801
Ca (mg/L)	2.14	6.23	6.07	1.13
Mg (mg/L)	0.88	0.60	0.98	0.23
Na (mg/L)	0.64	4.30	32.3	189
K (mg/L)	1.53	4.15	2.95	6.2
HCO_3 (mg/L)	11.5	14.5	62.7	155
CO_3 (mg/L)	–	–	12.0	133
Cl (mg/L)	1.65	2.60	1.7	4.7
SO_4 (mg/L)	–	0.93	13.7	51.9
Fe total (mg/L)	0.81	–	1.02	0.08
F (mg/L)	0.44	0.18	5.84	20.8
SiO_2 (mg/L)	–	14.0	16.0	29.1

– No analysis available

chemical characteristics of each aquifer zone, including the local stream water (A).

Water from the shallow aquifer (B) has low concentrations of Cl and SO_4 but considerable concentrations of K, Na, and Ca, and lower total dissolved solids (TDS) values than the other aquifer zones and a slightly acidic pH (from 5.4 to 6.9). Water tends to flow through the weathered zone to bedrock. Thus, water from the shallow aquifer zone chemically interacts with pyrite in the alkaline rocks, which removes oxygen from the water and creates more reducing conditions (Holmes et al. 1992).

The intermediate zone (C) is located at a depth of 150–200 m, with temperatures ranging from 21 to 26 °C. This zone differs from the shallower aquifer zone by its higher TDS content and its neutral to slightly alkaline pH (6.2–8.4). The groundwater in zone C is classified as bicarbonate with Ca and Na content.

The deep aquifer zone (D) is characterized by hyperthermal fluids (up to 40 °C) and an alkaline pH (≈ 9.6 to 9.8), with sodium-bicarbonate groundwater. This zone has higher TDS and higher concentrations of CO_3^{-2}, Na, SO_4^{-2}, and F^- ions than the shallower aquifer zones. The higher temperature increases the rock's rate of chemical dissolution and produces an enriched ion content, with notable F^- and SO_4^{-2} ions (Cruz and Peixoto 1989).

The creation of an open pit interfered in the original topography, lowering the water table and changing the groundwater dynamics. One of the most important chemical changes was the oxidation of dissolved sulfide to sulfate as the groundwater flowed upward.

Operational History and Tailings Management

The main facilities of the Osamu Utsumi Mine include the mine open pit, tailings impoundments, the processing plant for uranium extraction, waste rock piles, and administrative and operational support buildings (Fig. 2). The mine operated from 1981 to 1995, and uranium mining and milling operations ceased after depletion of the uranium ore. Its reserves have been estimated at ≈ 17,200 t of U_3O_8 (Fraenkel et al. 1985; Souza et al. 2013). About 1242 t of ammonium diuranate (yellowcake), 4.48×10^7 m^3 of waste material, and 2.39×10^6 m^3 of mine tailings were produced during the mine's operational years (Franklin 2007; Majdalani and Tavares 2001).

The cut-off grade was defined as 170 ppm of soluble U_3O_8 recovered from the processing plant; extracted material with lower grades was considered waste rock. Average and marginal ore production was 2500 and 1500 t/day, respectively, with a stripping ratio of 23.8 (Franklin 2007).

Ore beneficiation consisted of an acid leach using sulfuric acid in a proportion of 1 t of uranium ore to 70–150 kg of sulfuric acid to obtain ammonia diuranate [$UO_2(NO_3)_2 + NH_3 \rightarrow (NH_4)_2UO_7$] and molybdenum as calcium molybdate ($CaMoO_3$) (Franklin 2007). The leaching was conducted under controlled environmental conditions (70 °C) for 6 h (Cipriani 2002). After chemical leaching, filtering was used to separate solid and liquid components. The solid residue produced was washed with water to obtain a maximum uranium recovery and, after that, the washed solids were sent to the treatment plant (Cipriani 2002).

All effluents and solid waste generated by yellowcake production were sent to the wastewater treatment plant. Effluent treatment consisted of the neutralization of sulfuric acid with ground limestone to a pH of 9–10. Neutralization precipitated almost all iron and other metal ions (Al, Mg, Mn) as hydroxides. Likewise, the solid waste was composed of 98% low-grade uranium ore obtained by filtering, with a chemical treatment of neutralization with limestone. All waste produced from these methods was disposed in the tailings impoundment (Cipriani 2002).

Starting in 1998, the sludge produced by effluent and solid waste treatment was placed in the open pit, as depicted in Fig. 3. Its composition consisted mainly of metal hydroxides, such as Fe, Al, Mn, and radioactive elements, in a calcium sulfate matrix. This material is locally known as "DUCA" (for calcium diuranate) and includes the sludge produced by lime treatment of open-pit contact water and acid drainage from waste piles (Cipriani 2002).

Waste rock and tailings were disposed of in six piles and impoundments around the mining complex, the largest being BF-04 and BF-08 (Fig. 3). These piles are the two main sources of AMD. Since decommissioning began, groundwater has been monitored using wells installed around the CIPC and samples collected from the local drainage system to understand the extent of contamination over time (Fig. 3).

Structural and Geological Settings of BF-08 and the Study Area

The study area was part of the BF-08 tailings pile (Fig. 4), which covers an area of 64.4 million m^2, has a volume of 15 million m^3, 5 m wide benches, and 8 m long rocky slopes at an angle of 70°. The rocks in the pile are mainly composed of syenites and phonolites from the open pit area with an ore grade < 170 ppm and grain sizes ranging from fine sand (0.05–0.2 mm) to boulders (> 200 mm). The chemical composition is SiO_2 (55%), Al_2O_3 (21–23%), Fe (2.6%), F (1488–2013 ppm), Th (60–318 ppm), U (89–279 ppm), Zn (253–592 ppm), Zr (1009–1708 ppm), and S (5637–8616 ppm) (Waber 1992; Wiikmann 1998).

The tailings came from the picking and sorting of alkaline pyritic rocks (Cipriani 2002; Waber 1992). The material was end-dumped, so generally, fine grains remain at the top of the pile, whereas coarser cobbles and boulders are found in its basement.

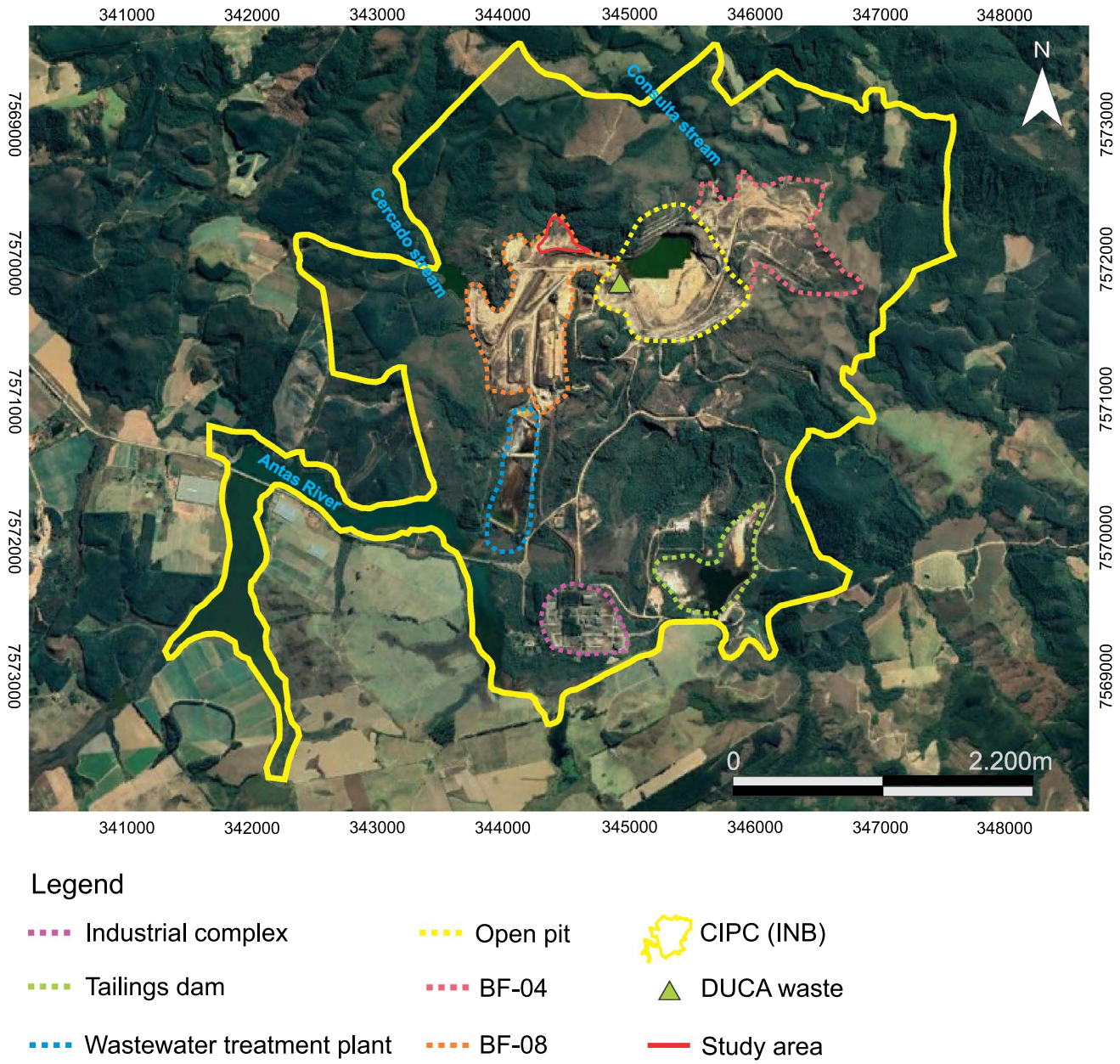

Fig. 2 Mining facilities of the Osamu Utsumi Mine

The BF-08 site is in the Cercado Stream watershed. The disposal area has a liner system to minimize upward flow into the tailings and improve the geotechnical stability of the impoundment. The drains consist of waste rock boulders covered with a finer-grained (clay) material also derived from waste rock, which acts like a liner below the tailings (Urânio do Brasil 1988). This system was developed to minimize possible interactions between the groundwater and tailings and minimize the movement of AMD into the groundwater.

The Cercado Stream had part of its channel diverted using tailings and waste rock for the new channel. The BF-08 site was covered with a 20 cm of clay with a slope between 0.5 and 1%. Rainwater run on was captured by concrete ditches and a piping system discharged the water to the local hydrological system. However, due to a lack of regular maintenance, the clay layer has been progressively eroded by rainwater, some ditches were damaged, and erosion has intensified on its slopes. As a result, neutral pH precipitation currently infiltrates into the pile and reappears downstream as acid drainage (Fig. 4) in a lake known as the BIA Reservoir. It is important to note that even though AMD is observed downstream, no contaminated seeps were observed to be issuing from the impoundment slopes in the study area.

Fig. 3 "DUCA," or chemical treatment plant sludge, disposed inside the open pit area and the monitoring wells PM-10 and PM-38 near the DUCA area (see Fig. 4 for locations)

Geophysical Methods and Data Acquisition

The geophysical investigations were carried out along seven lines to measure resistivity and chargeability (Fig. 5). The geophysical lines were parallel to each other and arranged 30 m apart, with a minimum length of 120 m (line 1), a maximum length of 340 m (line 7), and an electrode spacing of 5 m. DC resistivity and IP methods were applied using ERT and a Wenner-Schlumberger array. Thunderstorms, which could damage the equipment, are very common during the rainy season (October to March) in Brazil, so this study was conducted during the dry season (April to September).

The ABEM Terrameter LS resistivity meter (84 channels, 250 W, with a resolution of 1 µV, and a maximum current of 2.5A; ABEM 2012) that was used consists of a single module for transmission and receiving of automated signals to obtain resistivity and chargeability parameters simultaneously. The survey acquisition parameters settings were a signal sending time of 1.5 s, electrical current of 500 mA, two fixed reading windows of 100 ms, and 0.5 s of acquisition time delay. Non-polarizable porous-pot electrodes in a Cu-$CuSO_4$ solution were used to avoid local polarizations that would interfere with chargeability measurements during the IP survey.

The results from each geophysical line were analyzed using a data processing and inversion routine with Res2Dinv (2D) software, version 3.53 (Geotomo Software) to produce bidimensional sections with resistivity and chargeability values according to their distance from line origin and depth of acquisition. This software was designed to interpolate and invert field data from electrical geophysical prospecting according to the mathematical model of ordinary least squares (OLS). This technique smooths the extreme values using block modelling and reduces differences between measured and modeled parameters (Reynolds 2011). Resistivity inversion models required 5–7 iterations to obtain the most reliable 2D sections, whereas chargeability inversion models demanded 4–7 iterations, as indicated in each 2D section.

Block modelling generates a standard deviation parameter called the root mean squared (RMS) factor, which mainly represents the match between the calculated pseudo-section and that obtained in the field, influenced by the presence of extreme values in the input data, potentialized by post-processing (Chulès and Delfiner 2012; Geotomo 2003; Loke 2000). Resulting resistivity and chargeability models are presented as 2D sections with a chromatic logarithmic scale and intervals of interpolation in color values. This ERT data inversion routine is used in many kinds of studies, including mineral prospecting, hydrogeology, contaminated area diagnosis, and geotechnical engineering (Berthold et al. 2004; Camarero and Moreira 2017; Cavallari et al. 2018; Falgàs et al. 2011; Helene et al. 2016, 2020; Moreira et al. 2019; Silva et al. 2018; Vieira et al. 2016).

The geophysical surveys were planned to produce 3D visualization models by interpolation of the 2D sections, in addition to isovalue surfaces for resistivity and chargeability. This procedure was carried out using the Oasis Montaj

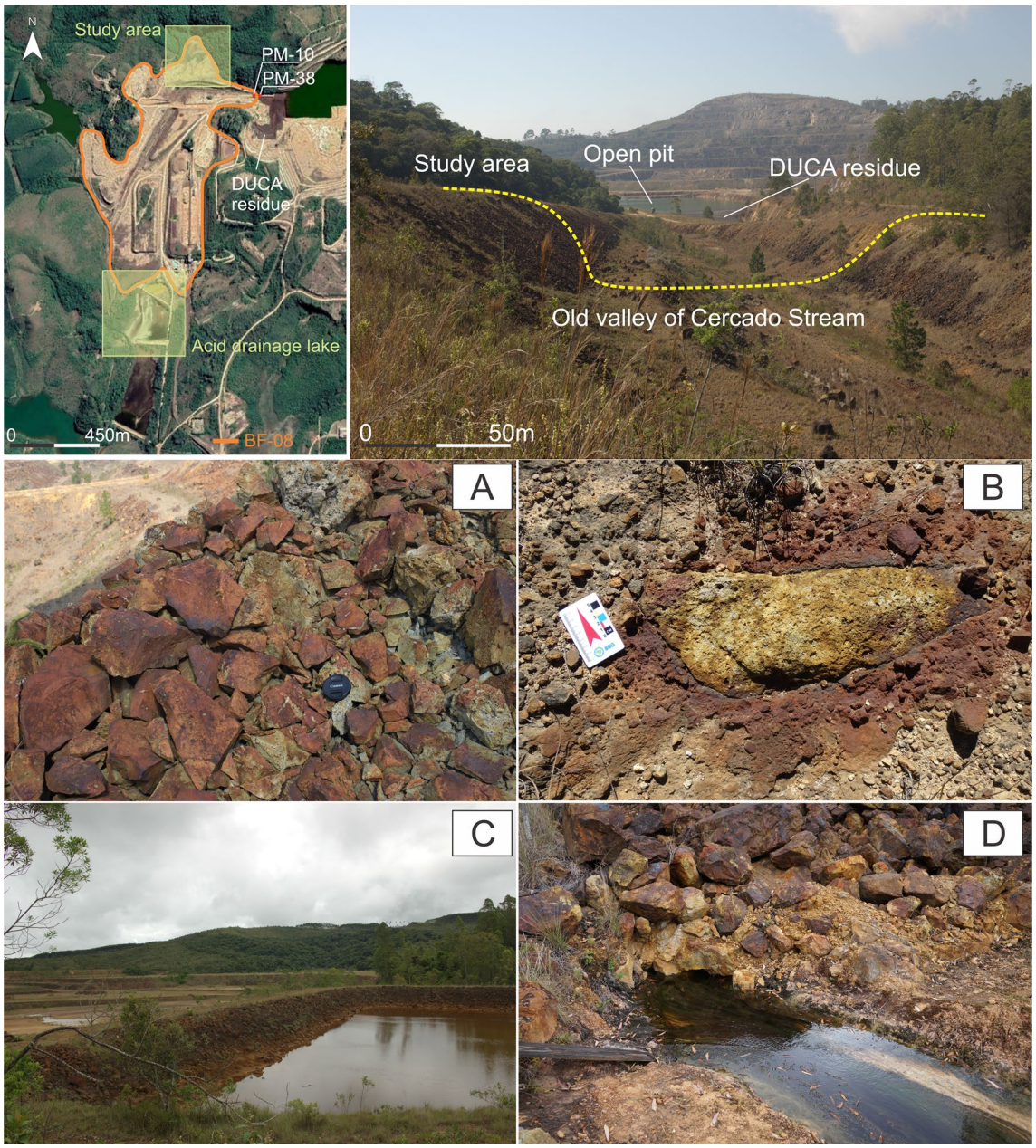

Fig. 4 Overview of BF-04 and its main geological and hydrogeological features: **A** oxidized rocks from the study area, **B** oxidized pyrite documented northeast of BF-08, **C** acid drainage lake formed at the toe of BF-08 (BIA Reservoir), and **D** acid drainage flowing from BF-08

Software Geosoft platform, which consisted of a tridimensional model created from coordinating data (X, Y, and Z) from the 2D sections (Geomotosoft 2014). Moreover, local topography was considered in all models to avoid distortions using the differential global positioning system. 3D modeling and isovalue surfaces improved the recognition and characterization of groundwater flow and sulfide zones, as well as AMD transport.

INB provided hydrochemical data from monitoring wells and surface water from 2015 to 2017 so that we could quantify chemical data and changes in physical–chemical parameters in groundwater. The nearest monitoring wells to the study area and the acid drainage lake located at the toe of BF-08 (the BIA Reservoir) were selected for chemical analysis of pH, electrical conductivity (EC), redox potential, dissolved oxygen (DO), turbidity, and major element chemistry (cations and anions). The hydrochemical data complemented the geophysical interpretations from BF-08 and helped identify the most critical AMD generation zones.

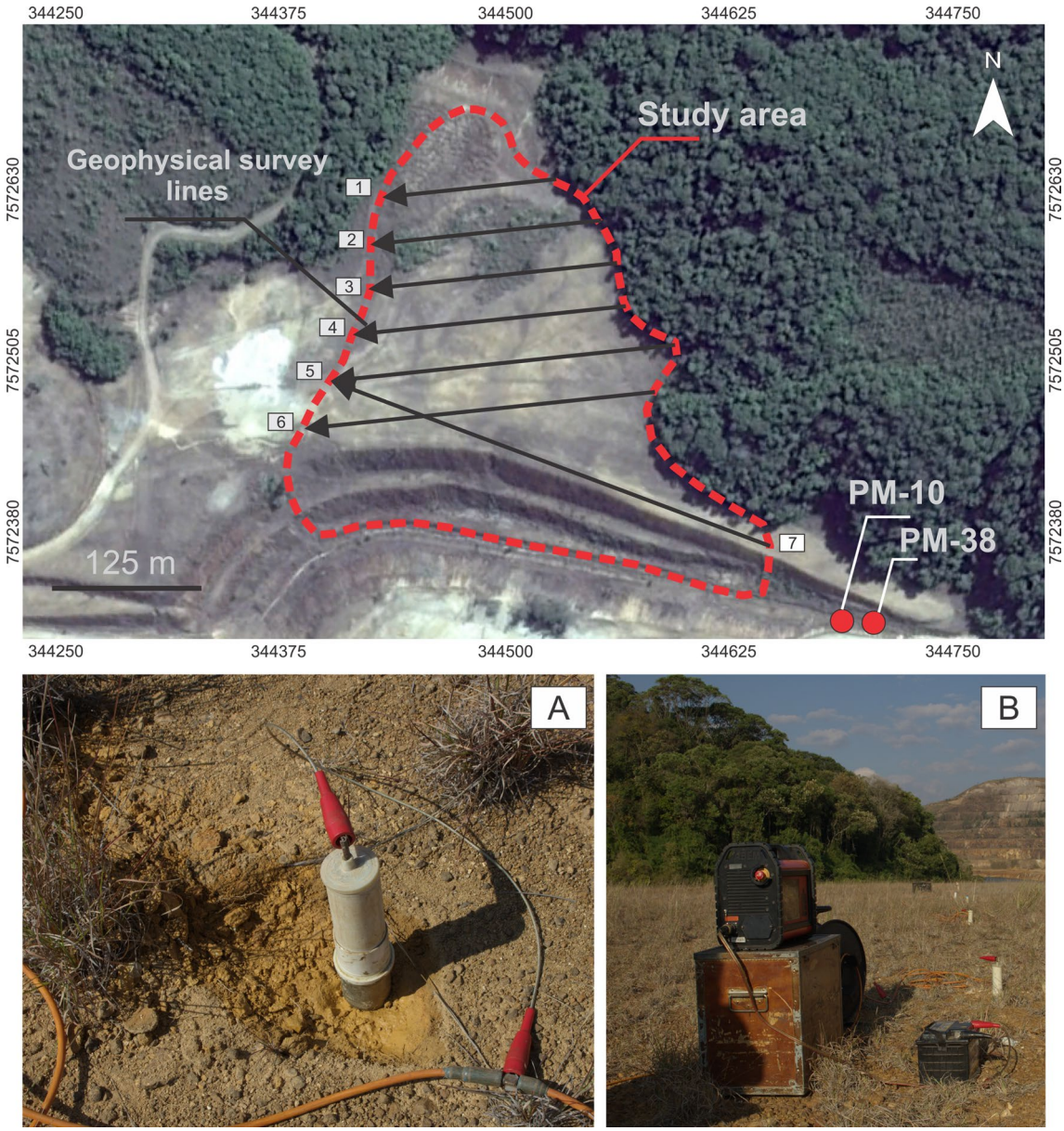

Fig. 5 Geophysical survey lines (top); **A** ABEM Terrameter LS resistivity meter and non-polarizable porous-pot electrodes, **B** equipment used to simultaneously measure resistivity and chargeability parameters

Groundwater samples were collected using the micro-purge low flow sampling method. First, monitoring wells went through a purging process to remove stagnant water, since this water cannot be considered as representative of the local aquifer quality. Then, sampling was performed using the micro-purge low flow method at flows of ≤ 0.5 L/min to minimize water table lowering (Popek 2018). This procedure ensures that the sample collected is consistent and representative of the contaminants in the local aquifer.

Chemical analyses were carried out by the INB team in partnership with CNEN (Brazilian Atomic Energy Commission) in the Poços de Caldas Laboratory (LAPOC/CNEN). The physical–chemical parameters were measured using a multiparameter probe coupled to a flow cell used in situ without filtration. Cations and anions were determined using plasma optical emission spectrometry (ICP-OES) in filtered samples that had been preserved with nitric acid. Sulfate was determined gravimetrically with barium chloride, and fluoride was determined using potentiometric analysis with an ion-specific electrode (Alberti 2017).

Results and Discussion

Geological materials have different resistance responses as electrical current passes through them. These responses can be quantified by considering the electrical current and voltage produced in the subsurface for each lithological setting. There are certain minerals, such as native metals and graphite, that are excellent electrical conductors, but most rock-forming minerals are insulating, and the passage of electrical current is only possible through dissolved ions dissolved in the water contained in their pores or fractures. The porosity thus plays a great role on the resistivity parameter, which tends to increase with decreasing porosity. Solutions with high ionic strength, and materials with metallic minerals and graphite, tend to have lower resistivity values and are generally represented by green and blue shades in geophysical cross-sections (Fig. 6). Zones with higher electrically resistivity, which include most rock-forming minerals, are represented by reddish and purple colors.

Besides electrical resistivity, chargeability is another parameter used in geophysical surveys to characterize the subsurface geological environment. This parameter is measured by induced polarization, which is based on the voltage stimulation that occurs after a delay in the transmission of artificial electric current in soil and rocks. The process is analogous to what occurs in a capacitor, whose cells are able to store energy and release it when the electrical source that powers the system ceases (Telford et al. 1990). As the current is interrupted, the difference in potential, which decays with time, is observed. The rate of this decay (induced polarization potential) depends on the geological nature of the investigated site, and factors such as rock lithology, pore geometry, and degree of saturation (Burtman and Zhdanov 2015).

The polarization phenomenon is more pronounced in rock with a high clay content and disseminated metallic minerals due to the membrane polarization effect. As electrical current flows through metallic minerals, it is possible to measure specific voltage and polarizability values for each mineral. In addition, there is a linear relationship between the maximum apparent chargeability and the concentration of sulfide minerals, which allows sulfide-rich zones to be identified (Wardlaw and Wagner 1994). In geophysical cross-sections, the regions with highly polarizable minerals (e.g. sulfides) are represented by purple and reddish colors, as seen in Fig. 7. It is important to note that the cross-sections in Figs. 6 and 7 are the opposite of those in Fig. 5 (i.e. west is to the right and east is to the left in Figs. 6 and 7).

The electrical properties of the geological subsurface are associated with its geometric parameters, such as thickness and depth, which informs local geological characterization. Since metals and metallic sulfides conduct electricity efficiently, electrical methods are important tools in the search for sulfide ores, as well as in environmental investigations involving metallic targets and groundwater prospecting.

Resistivity

The resistivity inversion models indicated a continuous low resistivity zone (< 74.6 Ω m) in lines 2–5 (blue areas in Fig. 6). As suggested by many studies (Alamry et al. 2017; Cardoso and Dias 2017; Kibria and Hossain 2012; Li et al. 2015; Targa et al. 2019), this geoelectrical layer was interpreted as a high ionic strength zone located 10 and 25 m below the surface.

The upper layers of BF-08 (to a 10 m depth) and those located below 35 m (yellow, orange, and red areas in Fig. 6) showed resistivity values exceeding 537 Ω m. This drastic change probably reflects hydraulic variations in the pile due to its construction method and the material used, which interferes with storage capacity and groundwater conductivity.

The clay-sized particles in the upper layers of the pile promote slower initial infiltration and water loss by evapotranspiration, which is indicated by high resistivity values in geophysical sections (Kibria and Hossain 2012; Ranjy et al. 2019). When deeper, more permeable layers are reached, as in the central region of the study area (lines 2–5), the groundwater enhances the leaching of sulfide minerals and other waste compounds.

Water flows towards the base of the pile where the boulders are present. This layer has higher porosity and permeability than the rest of the pile and lies above the bedrock, which is characterized by low permeability.

Another important aspect is the presence of zones with resistivity values < 20 Ω m on the western end of lines 5–7, 15 m below the surface, and on the eastern end of lines 3–7, 10–20 m deep (dark blue areas in Fig. 6). These lower resistivity values have been attributed to saturated zones with higher ionic strength, which favors electric current flow. Studies of Epov et al. (2017) and Maurya et al. (2017) demonstrated a strong correlation between low resistivity values (≈ 10 Ω m) and zones with active oxidation and leaching of geological material as sulfide minerals, which are intensified in acidic environments. These low resistivity zones are probably due to the oxidation of the sulfidic tailings in BF-08. Studies (e.g. Casagrande et al. 2020; Park et al. 2016) identified a correlation between the low resistivity anomalies and chemical weathering process in waste rock piles, and the presence of AMD.

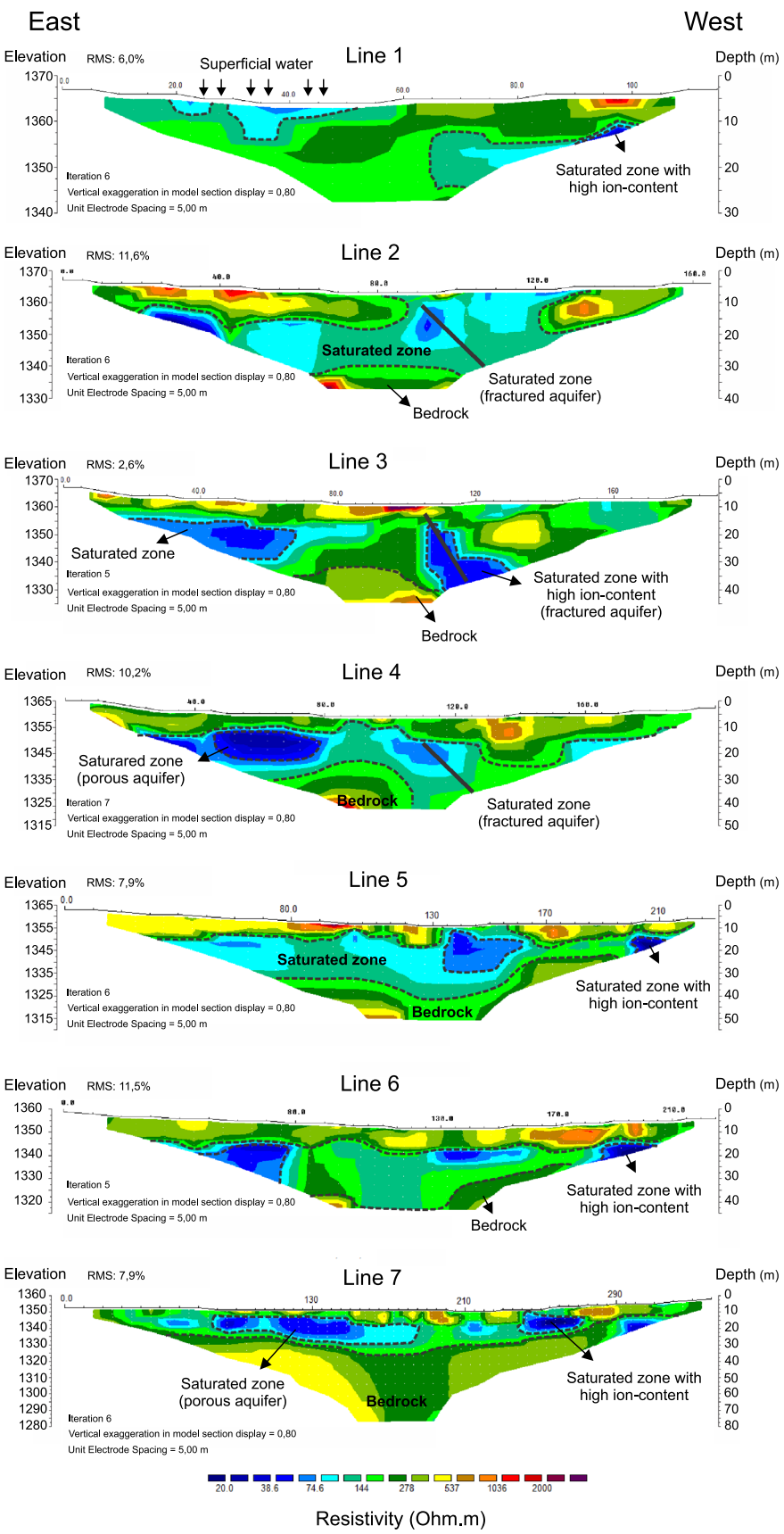

Fig. 6 2D inversion models that illustrate the contrast between zones with low resistivity values (blue shades) and high resistivity values (yellow and reddish shades). The black dashed lines outline saturated zones. Note that west is to the right and east is to the left in the 2D sections

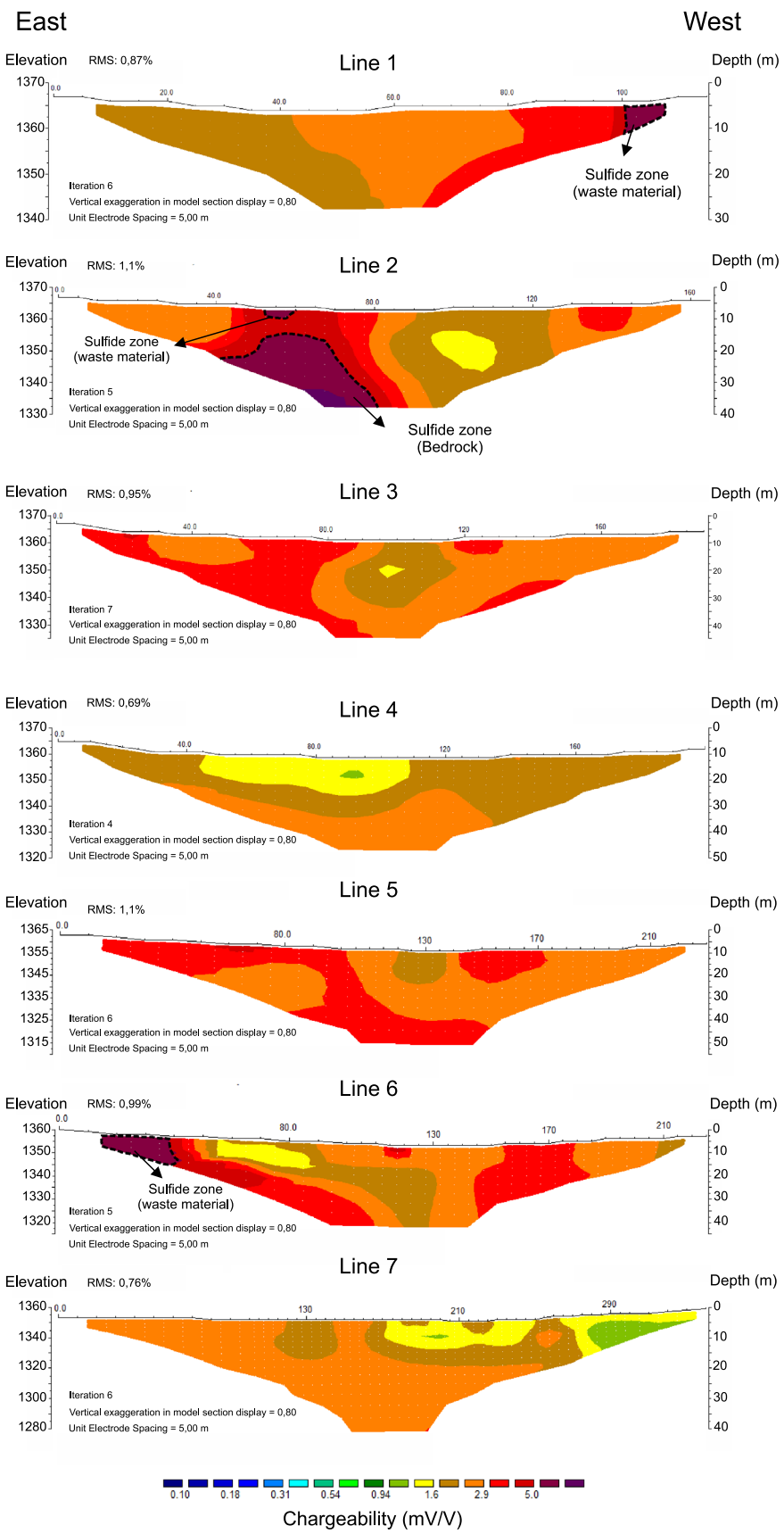

Fig. 7 2D inversion models indicating high chargeability zones (> 5.0 mV/V) interpreted as sulfide-rich waste materials and rocks

Chargeability

Chargeability inversion models showed more evidence of sulfide minerals in BF-08 (Fig. 7). It is possible to observe three high-chargeability anomalies (> 5.0 mV/V) located on the western side of line 1, at ≈ 10 m in depth, and at the east of lines 2 and 6 that extend from upper to basement layers of the tailings pile.

High chargeability values close to the surface were correlated with sulfide minerals in the waste materials and tailings that comprise the pile. On the other hand, anomalies located at deeper layers correspond to natural sulfide occurrences in the bedrock at depths below 35 m. There is a directly proportional relationship between chargeability and sulfide concentrations (Gurin et al. 2013; Hupfer et al. 2016; Kamura et al. 2019; Moreira et al. 2016, 2019; Rey et al. 2021). Yuval and Oldenburg (1996) demonstrated that maximum chargeability values (20 mV/V) were related to zones with a sulfide concentration of 4%, whereas poorly mineralized zones (< 1%) showed chargeability values from 0.1 to 0.4 mV/V. However, any quantitative comparison between different studies using the IP method must account for the acquisition parameters used in the fieldwork.

The resistivity inversion models also identified an anomaly in lines 2–4, which is highlighted in Fig. 6 by the black continuous lines located at the central-west part of these sections, near 25 m in depth. This anomaly is interpreted as groundwater flowing through fractures in the bedrock. Although absent in line 3, lines 2 and 4 illustrate that there is probably a hydrologic connection between the lower boulder layer of the tailings and the underlying fractured aquifer (bedrock). This hypothesis is corroborated by local hydrogeological studies that prove the presence of a porous aquifer in the weathered zone of alkaline rocks that is hydraulically connected to the underlying fractured aquifer system of unaltered nepheline-syenites (Nordstrom et al. 1992). Likewise, the tailings favor effluent percolation to the underlying aquifer.

The fact that the geophysical survey was carried out during the dry season may imply that the hydrologic connection between the tailings and the underlying aquifer systems is absent during the dry season due to water table lowering, as observed in line 3 (Fig. 6). During the rainy season, as the water table rises, it would restore the hydraulic connection between them. The raising and lowering of the water table throughout the year intensifies chemical weathering and AMD production (Nordstrom and Alpers 1999) and promotes the exchange of dissolved constituents from both systems. The fractured hydrogeological environment makes environmental remediation more difficult and complex.

Pseudo-3D Models

A pseudo-3D model was generated by the interpolation of the seven geophysical sections using the physical parameters of resistivity and chargeability to facilitate spatial visualization (Fig. 8). After data processing, images were smoothed, and visualization levels were defined using a specific depth range (Fig. 9).

Resistivity models from 12 to 32 m in depth corroborate interpretations obtained from the 2D models, which indicate a highly ionic effluent flowing from northeast to southwest and, therefore, a similar drainage pattern to the stream valley under the tailings pile. The contact between the tailings and bedrock is evident by a reduced number of saturated zones, with a resistivity > 537 Ω m. The water content decreases in part due to the presence of an elongated feature with high electrical resistance and N/S orientation, which is interpreted as the top of the bedrock with increasing resistivity values with depth (> 2000 Ω m from 42 m in depth), interrupting the connection between the saturated and unsaturated zones.

Visualization levels also indicated specific locations where there is clear evidence of effluents flowing from the tailings towards the underlying fractured aquifer. The existence of a low resistivity zone in the southeast portion of the pseudo-3D model (Fig. 9), towards the open pit area, is another indication that local aquifers could be hydraulically connected, with acidic effluent flowing through the fracture system. Another feature observed was a NW–SE alignment, highlighted at 42 and 62 m depths in Fig. 9, indicating a fractured zone that transports water into the bedrock.

The DUCA residue inside the open pit area close to BF-08 is potentially problematic. Water from the old exploration areas and the local water table will interact with this residue and transport contaminants toward the fractured aquifer. Consequently, this contaminated effluent infiltrates into the deepest part of the aquifer through the local fracture system and, as the water table rises, it flows toward the porous portion of BF-08.

Another tool that helped in the geophysical data visualization was the resistivity and chargeability pseudo-3D isovalue modeling (Fig. 10). It was created to highlight the low resistivity zones (with values < 20 Ω m) and on top of that, a chargeability interpolation to visualize the 3D distribution of the sulfidic areas. As depicted in Fig. 10, sulfide zone 1 is mostly concentrated from the surface to depths of 15 m in BF-08, which includes tailings and waste rock. In sulfide zone 3, sulfide minerals are concentrated at a greater depth in the tailings and bedrock. Sulfide zone 2 has a homogenous distribution of sulfide minerals from the tailings and bedrock.

Combining both models, it is possible to observe a strong interaction between zone 3 and water retained

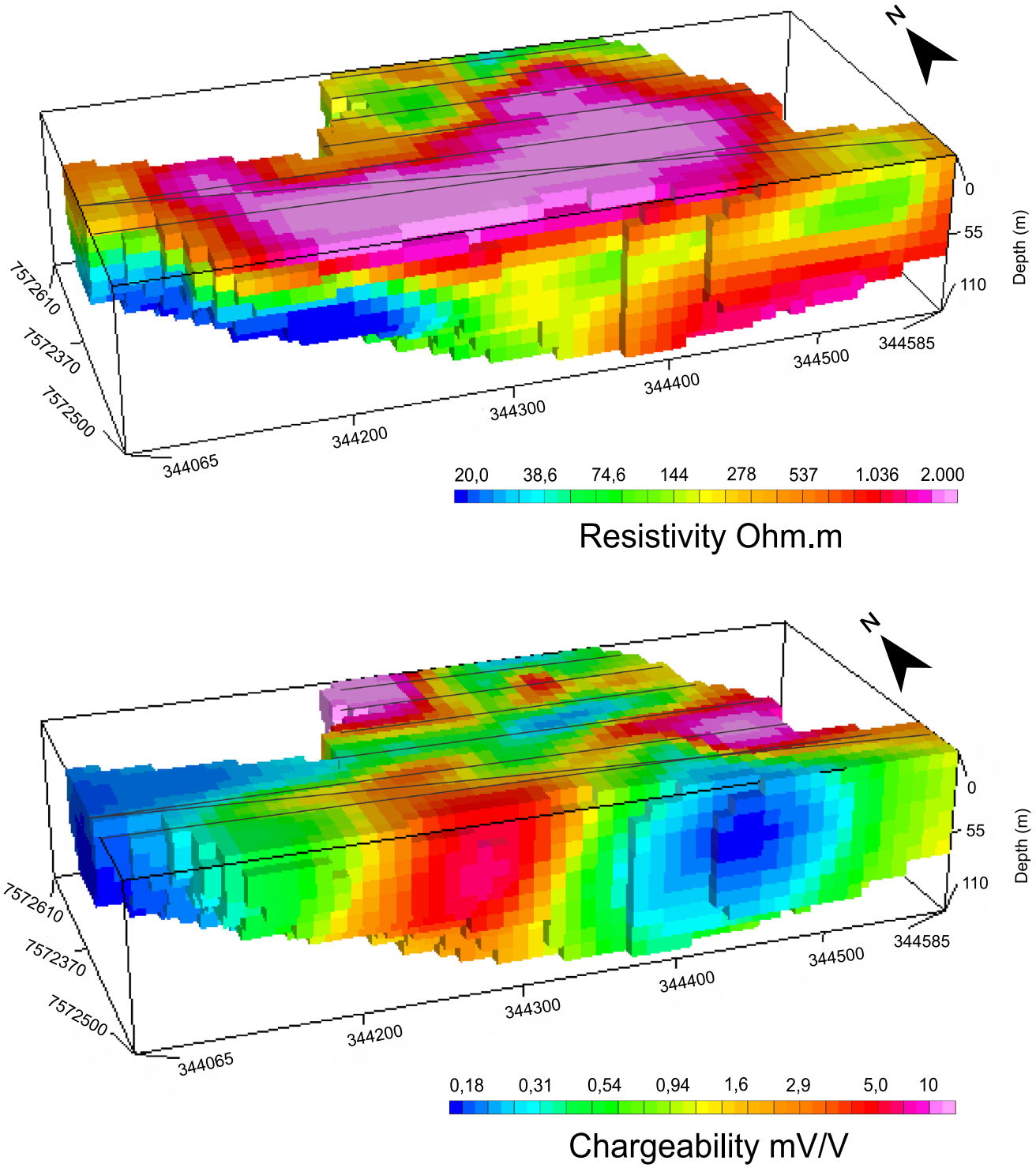

Fig. 8 3D visualization models created from 2D section interpolation considering resistivity (above) and chargeability (below) parameters

inside the pile, with a high potential for AMD generation. The presence of saturated zones with resistivity values < 20 Ω m is a strong indication that chemical weathering and leaching of sulfide minerals is active and

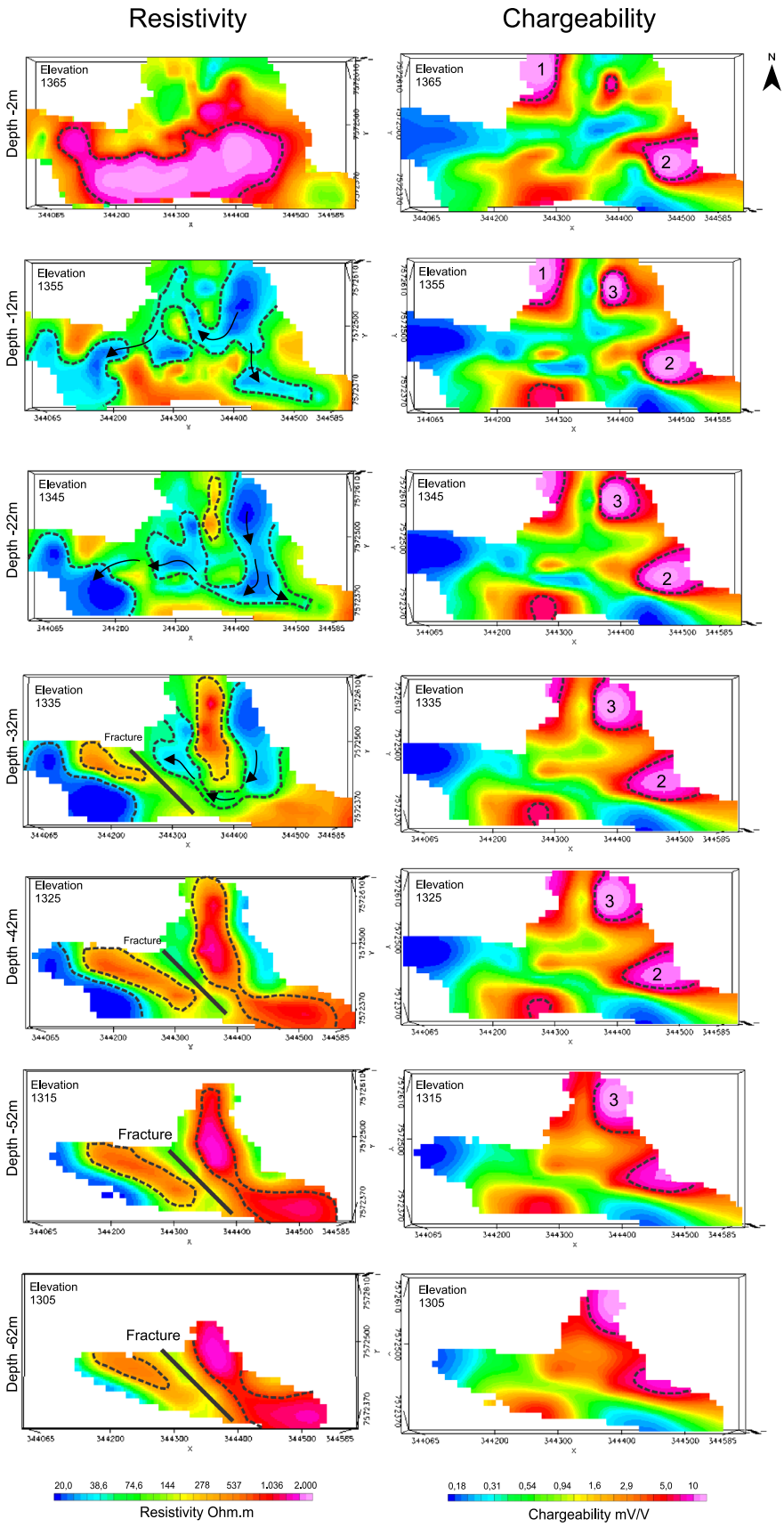

Fig. 9 Visualization levels from 2 and 62 m depth and geophysical interpretation based on the resistivity and chargeability 3D models

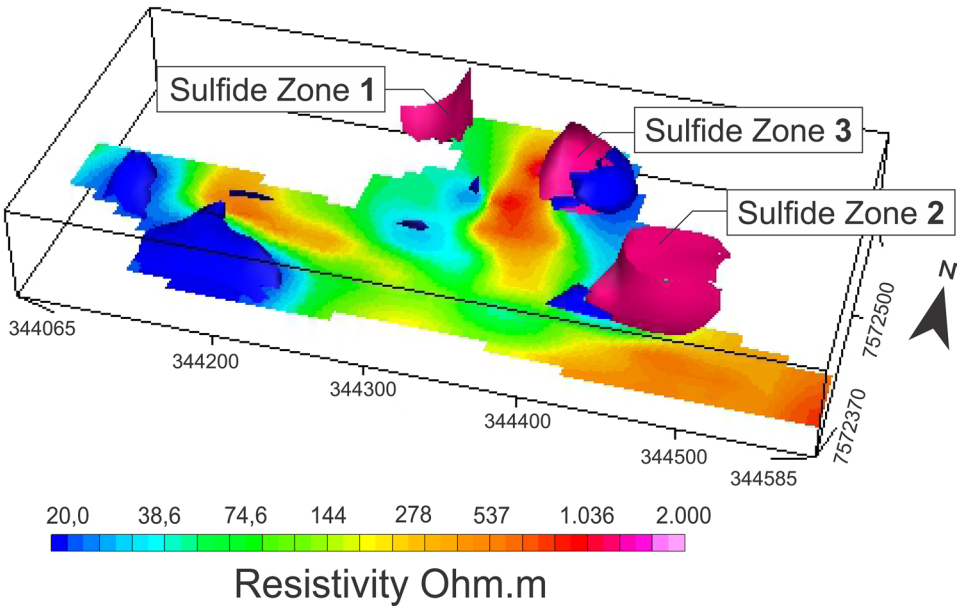

Fig. 10 Pseudo-3D isovalue modeling created from resistivity values, highlighting values lower than 20 Ω m (dark blue shades), and on top of that a chargeability values interpolation higher than 5 mV/V to provide a 3D visualization of the 3 sulfide areas (colored in pink and numbered from 1 to 3). Sulfide zone 1 is mostly concentrated at the shallower layers of BF-08 whereas Sulfide zone 2 shows a homogenous distribution of sulfide minerals and sulfide zone 3 is presented in the deeper layers of the tailings and bedrocks

producing a higher concentration of dissolved ions, especially sulfate.

Hydrochemistry

The hydrochemical data complemented geophysical interpretations to characterize the hydrogeological environment of BF-08 (Table 2). Data from monitoring wells PM-10 and PM-38 indicated distinct physical–chemical characteristics of local groundwater. These wells were installed at 8 m and 25 m deep, respectively. Thus, PM-10 reflects chemical conditions in the tailings, whereas PM-38 gives chemical information about the underlying fractured aquifer, assuming its well casing prevents influence from the overlying tailings.

The tailings water had an acidic pH (4.50–4.66), higher concentrations of DO (2.81–4.67 mg/L), mostly positive redox potentials (oxidizing environment), and low EC values (50–93 µS/cm). The deeper zones had a more reducing environment, with slightly acidic to neutral pH (5.37–6.86), lower concentrations of DO (0.45–2.2 mg/L), and higher

Table 2 Analytical results of groundwater samples collected from PM-10 and PM-38 and surface water from the BIA Reservoir provided by INB

	Date	pH	Turb[a]	EC[b]	DO[c]	T[d]	WT[e]	Eh	Al (mg/L)	Fe (mg/L)	Mn (mg/L)	Sulfate (mg/L)	Fluoride (mg/L)
PM 10	Apr/2015	4.5	3.2	83	3.85	19.2	691	409	1.9	0.19	2.34	48.6	–
	Oct/2015	4.62	5	93	2.81	18.9	715	256	2.1	–	2.08	37.7	1.61
	Oct/2017	4.66	48	50	4.67	18.8	728	240	1.03	0.08	0.83	17.8	–
PM 38	Jan/2016	6.86	15.6	707	0.49	20.8	838	59	0.1	0.01	0.3	139	2.44
	Oct/2017	6.83	21.1	620	1.18	19.3	897	− 11	0.07	0.13	1.63	257	3.5
BIA	Nov/2015	5.52	5.5	1228	3.49	19.8	770	299	76.8	18.6	49.0	942	43.3
	Oct/2017	3.76	431	1450	1.16	19.9	740	308	154	31.4	86.4	1280	47.0

PM-10 was installed at 8 m depth and gives information about the hydrochemical conditions of the upper layers of BF-08. PM-38 is screened at 25 m deep and reflects the hydrochemical environment of the underlying aquifer. BIA Reservoir describes the hydrochemical conditions of the lake downstream of BF-08

INB Nuclear Industries of Brazil (Indústrias Nucleares do Brasil)

– No results available

[a]Turbidity NTU

[b]Electrical conductivity (µS/cm)

[c]Dissolved oxygen (mg/L)

[d]Temperature (°C)

[e]Water table depth (cm)

EC values close to the open pit area (360–707 µS/cm), in addition to high sulfate concentrations.

The water sample from BIA Reservoir had the most acidic pH (3.76) and the highest EC (1228–1450 µS/cm) (Table 2). Analytical results indicated higher concentrations in the BIA Reservoir than in the monitoring wells. Sulfate dominates the sample, reflecting the oxidation of sulfide minerals in BF-08. The acidic water enhances the chemical mobility of metals and explains the higher Al, Fe, and Mn concentrations.

Because groundwater sampling was in the upper layer of the local aquifer system, it was expected that the water quality would be similar to that observed in the shallow aquifer zone (B), as described in Table 1. However, the sample from the upper fractured aquifer (PM-38, Table 2) has higher SO_4 and F concentrations and a slightly acidic pH compared to the background levels in the regional aquifer (Sample B, Table 1).

Although the tailings have favorable conditions for acid generation and considerable potential to modify contaminant mobility inside the tailings, the fractured aquifer had higher sulfate concentrations, which was unexpected (Baruah and Khare 2010; Jardim 2014). Thus, it is possible that external factors might affect the chemical composition of the tailings water, including the possible dissolution of DUCA residues from inside the open pit. It is believed that the DUCA residue dissolves, infiltrates into the bedrock through fractures, and is dispersed into the entire fractured aquifer. The DUCA contaminants apparently are not restricted to the fractured hydrogeological environment. As shown in 2D and pseudo-3D models, the tailings and underlying fractured aquifer are hydraulically connected, which allows effluent circulation. In other words, in addition to acid drainage generated inside BF-08, the tailings could be impacted by contaminants from the DUCA residue.

Conclusions

The results of the geophysical study provided a good understanding of the hydrogeological dynamics and underground flow of AMD inside the tailings impoundment at BF-08, as well as the identification of sulfidic zones. It was possible to distinguish less impacted saturated zones (< 74.6 Ω m) from those with high ion content probably related to AMD (< 20 Ω m), as well as three sulfide mineralization and high resistivity areas indicating the boundary between the base of the tailings in BF-08 and the top of the bedrock at ≈ 35 m deep. The inversion model suggests a possible hydraulic connection between the tailings and the underlying fractured aquifer that favors chemical exchanges between them. The 3D visualization models showed that the mineralized area of BF-08 is susceptible to chemical weathering and leaching and, hence, to generating AMD due to its interaction with saturated zones.

The hydrochemical data corroborated the geophysical interpretation and indicates the existence of two hydrogeological systems. The tailings material has characteristics that allow chemical weathering and leaching due to high concentrations of DO and an acidic pH. The combination of these two parameters provide ideal conditions to dissolve and mobilize constituents within the pile, such as Fe, Al, Mn, and S, and indicates that the tailings are a source of groundwater contamination.

Although the groundwater in the fractured aquifer does not have a chemical signature compatible with acid drainage, the higher concentration of sulfate could reflect impacts from the dissolution and transport of contaminants from the DUCA residue. This residue could release contaminants that infiltrate into the bedrock through fractures and affect the regional aquifer system.

Using the combined geophysical and hydrochemical results, it was possible to identify a transition zone below the overlying oxidizing zone in the tailings where leaching of sulfide minerals is intensified, which could provide high concentrations of dissolved ions to the underlying more-reducing groundwater. The tailings areas with high sulfide content should be especially targeted during remediation because they have a high potential to generate acid drainage. Thus, the integrated analysis of DC resistivity and IP methods provided an improved understanding of in situ mitigation measures that could be used to more successfully minimize and control releases during the decommissioning and closure of mining complexes.

Acknowledgements The authors thank the São Paulo Research Foundation (FAPESP) for funding the project "Study of the acid mine drainage generation in uranium mine tailings" (nº 2019/14565-3), the National Council for Scientific and Technological Development (CNPq) for financial support, and the INB for collaborating and allowing the development of fieldwork, with technical support, and access to data and the study area.

References

ABEM (2012) Terrameter LS—Instruction manual. ABEM Instrument, Sundbyberg, Sweden

Akcil A, Koldas S (2006) Acid Mine Drainage (AMD): causes, treatment and case studies. J Clean Prod 14:1139–1145. https://doi.org/10.1016/j.jclepro.2004.09.006

Alamry AS, van der Meijde M, Noomen M, Addink E, van der Benthem R, Jong SM (2017) Spatial and temporal monitoring of soil moisture using surface electrical resistivity tomography in Mediterranean soil. CATENA 157:388–396. https://doi.org/10.1016/j.catena.2017.06.001

Alberti HL (2017) Estudo hidroquímico e isotópico das águas subterrâneas impactadas pela drenagem ácida da mina de urânio—Osamu Utsumi, Planalto de Poços de Caldas (MG). Thesis, State Univ of Campinas (**in Portuguese**)

Anterrieu O, Chouteau M, Aubertin M (2010) Geophysical characterization of the large-scale internal structure of a waste rock pile from a hard rock mine. Bull Eng Geol Environ 69:533–548. https://doi.org/10.1007/s10064-010-0264-4

Armstrong M, Petter R, Petter C (2019) Why have so many tailings dam failed in recent years? Resour Policy 63:101412. https://doi.org/10.1016/j.resourpol.2019.101412

Aubertin M (2013) Waste rock disposal to improve the geotechnical and geochemical stability of piles. World Mining Congress. Montreal

Baruah BP, Khare P (2010) Mobility of trace and potentially harmful elements in the environment from high sulfur Indian coal mines. Appl Geochem 25:1621–1631. https://doi.org/10.1016/j.apgeochem.2010.08.010

Berthold S, Bentley LR, Hayashi M (2004) Integrated hydrogeological and geophysical study of depression focused groundwater recharge in the Canadian prairies. Water Resour Res 40:1–14. https://doi.org/10.1029/2003WR002982

Bortnikova S, Olenchenko V, Gaskova O, Yurkevich N, Abrosimova N, Shevko E, Edelev A, Korneeva T, Provornaya I, Eder L (2018) Characterization of a gold extraction plant environment in assessing the hazardous nature of accumulated waste (Kemerovo region, Russia). Appl Geochem 93:145–157. https://doi.org/10.1016/j.apgeochem.2018.04.009

Burtman V, Zhdanov MS (2015) Induced polarization effect in reservoir rocks and its modeling based on generalized effective-medium theory. Resour Effic Technol 1:34–48. https://doi.org/10.1016/j.reffit.2015.06.008

Camarero PL, Moreira CA (2017) Geophysical investigation of earth dam using the electrical tomography resistivity technique. Int Eng J 70:47–52. https://doi.org/10.1590/0370-44672016700099

Cardoso R, Dias AS (2017) Study of the electrical resistivity of compacted kaolin based on water potential. Eng Geol 226:1–11. https://doi.org/10.1016/j.enggeo.2017.04.007

Casagrande MFS, Moreira CA, Targa DA, Alberti HLC (2018) Integration of geophysical methods in the study of acid drainage in uranium mining waste. Braz J Geophys 36(4):439–450. https://doi.org/10.22564/rbgf.v36i4.1968

Casagrande MFS, Moreira CA, Targa DA (2020) Study of generation and underground flow of acid mine drainage in waste rock pile in uranium mine using electrical resistivity tomography. Pure Appl Geophys 77:703–721. https://doi.org/10.1007/s00024-019-02351-9

Cathles LM, Shea ME (1992) Near-field high temperature transport: evidence from the genesis of the Osamu Utsumi uranium mine, Poços de Caldas alkaline complex, Brazil. J Geochem Explor 45:565–603

Cavallari F, Moreira CA, Helene LPI (2018) Environmental geophysical diagnosis of a contaminated area by hydrocarbon in a railway accident in the municipality of Botucatu-SP, Brazil. Braz J Geophys 36:527–540

Chulès JP, Delfiner P (2012) Geostatistics—modeling spatial uncertainly. Wiley, Hoboken

Cipriani M (2002) Mitigação dos impactos sociais e ambientais decorrentes do fechamento definitivo de minas de urânio. Thesis, State Unive of Campinas (**in Portuguese**)

Costa PCG, Delgado SL, Carmos JCC (1998) Projeto hidrogeoambiental das estâncias hidrominerais da companhia mineradora de Minas Gerais (COMIG). Technical Report COMIG/Fundação Gorceix, 69p (**in Portuguese**)

Cruz WB, Peixoto CAM (1989) As águas termais de Poços de Caldas, MG—Estudo experimental das interações água-rocha. Revista Brasileira De Geociências 19:76–86 (**in Portuguese**)

Dawood I, Aubertin M (2014) Effect of dense materials layers on unsaturated water flow inside a large waste rock pile: a numerical investigation. Mine Water Environ 33:24–38. https://doi.org/10.1007/s10230-013-0251-7

Dutta M, Islam N, Rabha S, Narzary B, Bordoloi M, Saikia D, Silva LFO, Saikia BK (2020) Acid mine drainage in an Indian high-sulphur coal mining area: cytotoxicity assay and remediation study. J Hazard Mater 389:121851. https://doi.org/10.1016/j.jhazmat.2019.121851

Epov MI, Yurkevich NV, Bortnikova SB, Karin YG, Saeva OP (2017) Analysis of mine waste by geochemical and geophysical methods (a case study of the mine tailing dump of the Salair ore processing plant). Russ Geol Geophys 58:1543–1522. https://doi.org/10.1016/j.rgg.2017.11.014

Equeenuddin SM, Trpathy S, Sahoo PK, Panigrahi MK (2013) Metal behavior in sediment associated with acid mine drainage stream: role of pH. J Geochem Explor 124:230–237. https://doi.org/10.1016/j.gexplo.2012.10.010

Fala O, Aubertin M, Molson J, Bussière B, Wilson GW, Chapuis RP, Martin V (2003) Numerical modeling of unsaturated flow in uniform and heterogeneous waste rock piles. In: Proceedings of the 6th international conference on acid rock drainage (ICARD), pp 895–902

Falgàs E, Ledo J, Benjumea B, Queralt P, Marcuello A, Teixidó T, Martí A (2011) Integrating hydrogeological and geophysical methods for the characterization of a deltaic aquifer system. Surv Geophys 32:857–873. https://doi.org/10.1007/s10712-011-9126-2

Fraenkel MO, Santos RC, Loureiro FEVL, Muniz WS (1985) Jazidas de urânio no Planalto de Poços de Caldas—Minas Gerais. Principais minerais do Brasil, vol 1. MMe, DNPM e CVRD, pp 89–103 (**in Portuguese**)

Franklin MR (2007) Modelagem numérica do escoamento hidrológico e dos processos geoquímicos aplicados à previsão da drenagem ácida em uma pilha de estéril da mina de urânio de Poços de Caldas—MG. Thesis, Federal Univ of Rio de Janeiro (**in Portuguese**)

Freitas APP, Schneider IAH, Schwartzbold A (2011) Biosorption of heavy metals by algal communities in water streams affected by the acid mine drainage in the coal mining region of Santa Catarina State, Brazil. Miner Eng 24:1215–1218. https://doi.org/10.1016/j.mineng.2011.04.013

Geomotosoft (2014) Oasis Montaj: how to guide. http://updates.geosoft.com/downloads/files/how-to-guides/Oasis_montaj_Gridding.pdf

Geotomo software (2003) Geoelectrical imaging 2D & 3D. https://www.geotomosoft.com/downloads.php

Glotov VE, Chlachula J, Glotova LP, Little E (2018) Causes and environmental impact of the gold tailings dam failure at Karamken, the Russian Far east. Eng Geol 245:236–247. https://doi.org/10.1016/j.enggeo.2018.08.012

Golder Associates (2012) Plano de Recuperação de Áreas Degradas—INB UTM Caldas. Technical report, Belo Horizonte

Gurin G, Tarasov A, Ilyin Y, Titotv K (2013) Time domain spectral induced polarization of disseminated electronic conductor: laboratory data analysis through the Debye decomposition approach. J Appl Geophys 98:44–53. https://doi.org/10.1016/j.jappgeo.2013.07.008

Helene LPI, Moreira CA, Carrazza LP (2016) Applied geophysics on a soil contaminated site by chromium of a tannery in Motuca (SP, Brazil). Braz J Geophys 34:309–317. https://doi.org/10.22564/rbgf.v34i3.825

Helene LPI, Moreira CA, Bovi RC (2020) Identification of leachate infiltration and its flow pathway in landfill by means of electrical resistivity tomography (ERT). Environ Monit Assess 192(249):1–10. https://doi.org/10.1007/s10661-020-8206-5

Holmes DC, Pitty AE, Noy DJ (1992) Geomorphological and hydrogeological features of the Poços de Caldas caldera analogue study sites. J Geochem Explor 45:215–247. https://doi.org/10.1016/0375-6742(92)90126-S

Hupfer S, Martin T, Weller A, Günther T, Huhn K, Ngninjio VDN, Noell U (2016) Polarization effects of unconsolidated sulphide-sand-mixtures. J Appl Geophys 135:456–465. https://doi.org/10.1016/j.jappgeo.2015.12.003

Jardim WF (2014) Medição e interpretação de valores do potencial redox (Eh) em matrizes ambientais. Quim Nova 37:1233–1235. https://doi.org/10.5935/0100-4042.20140207 (**in Portuguese**)

Kamura K, Omori M, Kurokawa M, Tanaka H (2019) Estimation of the potential of landfill mining and exploration of metal enriched zones. Waste Manag 93:122–129. https://doi.org/10.1016/j.wasman.2019.04.050

Kibria G, Hossain MS (2012) Investigation of geotechnical parameters affecting electrical resistivity of compacted clays. J Geotech Geoenviron Eng 138:1520–1529. https://doi.org/10.1061/(ASCE)GT.1943-5606.0000722

Lei L, Watkins R (2005) Acid drainage reassessment of mining tailings, Black Swan Nickel Mine, Kalgoorlie, Western Australia. Appl Geochem 20:661–667. https://doi.org/10.1016/j.apgeochem.2004.09.011

Li S, Liu B, Nie L, Liu Z, Tian M, Wang S, Su M, Guo Q, (2015) Detecting and monitoring of water inrush in tunnels and coal mines using direct current resistivity method: a review. J Rock Mech Geotech Eng 7:469–478. https://doi.org/10.1016/j.jrmge.2015.06.004

Loke MH (2000) Electrical imaging surveys for environmental and engineering studies. A practical guide to 2-D and 3-D surveys. Res2Dinv Manual. IRIS Instruments. www.iris-instruments.com

Majdalani AA, Tavares AM (2001) Status of uranium in Brazil. IAEA—TECDOC 1258, IAEA, Vienna, pp 119–127

Martín-Crespo T, Gómes-Ortiz D, Marín-Velázquez S, Martínez-Pagán P, Ignacio C, Lillo J, Faz A (2018) Geoenvironmental characterization of unstable abandoned mine tailings combining geophysical and geochemical methods (Cartagena-La Union district, Spain). Eng Geol 232:135–146. https://doi.org/10.1016/j.enggeo.2017.11.018

Martínez-Pagán P, Gómez-Ortiz D, Martín-Crespo T, Martín-Velázquez S, Martínez-Segura M (2021) Electrical resistivity imaging applied to tailings ponds: an overview. Mine Water Environ. https://doi.org/10.1007/s10230-020-00741-3

Maurya PK, Ronde VK, Fiandaca G, Balbarini N, Auken E, Bjerg PL, Christiansen AV (2017) Detailed landfill leachate plume mapping using 2D and 3D electrical resistivity tomography—with correlation to ionic strength measured in screens. J Appl Geophys 138:1–8. https://doi.org/10.1016/j.jappgeo.2017.01.019

Migaszewski ZM, Galuszka A, Dolegowska S (2018) Extreme enrichment of arsenic and rare Earth elements in acid mine drainage: case study of Wisniowka mining area (south-central Poland). Environ Pollut 244:898–906. https://doi.org/10.1016/j.envpol.2018.10.106

Moreira CA, Borssatto K, Ilha LM, Santos SF, Rosa FTG (2016) Geophysical modeling in gold deposit through DC resistivity and induced polarization methods. Int Eng J 69(3):293–299. https://doi.org/10.1590/0370-44672016690001

Moreira CA, Santos EG, Ilha LM, Paes RAS (2019) Recognition of sulfides zones in marble mine through comparative analysis of electrical tomography arrangements. Pure Appl Geophys 176:4907–4920. https://doi.org/10.1007/s00024-019-02243-y

Moreno GR, Cánovas CR, Olías M, Macías F (2020) Seasonal variability of extremely metal rich acid mine drainages from the Tharsis mines (SW Spain). Environ Pollut 259:113829. https://doi.org/10.1016/j.envpol.2019.113829

Moyé J, Picard-Lesteven T, Zouhri L, Amari KE, Hibti M, Benkaddour A (2017) Groundwater assessment and environmental impact in the abandoned mine of Kettara (Morocco). Environ Pollut 231:899–907. https://doi.org/10.1016/j.envpol.2017.07.044

Naicker K, Cukrowska E, Mccarthy TS (2003) Acid mine drainage arising from gold mining activity in Johannesburg, South Africa and environs. Environ Pollut 122:29–40. https://doi.org/10.1016/S0269-7491(02)00281-6

Nordstrom DK, Alpers CN (1999) Geochemistry of acid mine waters. In: Plumlee GS, Logsdon MJ (eds) Chapter 6, The environmental geochemistry of mineral deposits. Society of Economic Geologists, Littleton, pp 133–160

Nordstrom DK, Mcnutt RH, Puigdomènech I, Smellie JAT, Wolf M (1992) Groundwater chemistry and geochemical modeling of water-rock interactions at the Osamu Utsumi mine and the Morro do Ferro analogue study sites, Poços de Caldas, Minas Gerais, Brazil. J Geochem Explor 45:249–287. https://doi.org/10.1016/0375-6742(92)90127-T

Nordstrom DK, Blowes DW, Ptacek CJ (2015) Hydrogeochemistry and microbiology of mine drainage: an update. Appl Geochem 57:3–16. https://doi.org/10.1016/j.apgeochem.2015.02.008

Olenchenko VV, Kucher DO, Bortnikova SB, Gas'kova OL, Edelev AV, Gora MP (2016) Vertical and lateral spreading of highly mineralized acid drainage solutions (Ur dump, Salair): electrical resistivity tomography and hydrogeochemistal data. Russ Geol Geophys 57:617–628. https://doi.org/10.1016/j.rgg.2015.05.014

Owen JR, Kemp D, Svobodova K, Pérez MG (2020) Catastrophic tailings dam failures and disaster risk disclosure. Int J Disaster Risk Reduct 42:101361. https://doi.org/10.1016/j.ijdrr.2019.101361

Pabst T, Bussière B, Aubertin M, Molson J (2018) Comparative performance of cover systems to prevent acid mine drainage from pre-oxidized tailings: a numerical hydrogeochemical assessment. J Contam Hydrol 214:39–53. https://doi.org/10.1016/j.jconhyd.2018.05.006

Park I, Tabelin CB, Jeon S, Li X, Seno K, Ito M, Hiroyoshi N (2016) A review of recent strategies for acid mine drainage prevention and mine tailings recycling. Chemosphere 219:588–606. https://doi.org/10.1016/j.chemosphere.2018.11.053

Popek E (2018) Sampling and analysis of environmental chemical pollutants. Chapter 4, Practical approach of sampling, 2nd edn. Elsevier, pp 145–225

Power C, Tsourlos P, Ramasamy M, Nivorlis A, Mkandawire M (2018) Combined DC resistivity and induced polarization (DC-IP) for mapping the internal composition of a mine waste rock pile in Nova Scotia, Canada. J Appl Geophys 150:40–51. https://doi.org/10.1016/j.jappgeo.2018.01.009

Ranjy RH, Hafizi MK, Kermani MRS, Nik MRG (2019) Electrical resistivity method for water content and compaction evaluation, a laboratory test on construction material. J Appl Geophys 168:49–58. https://doi.org/10.1016/j.jappgeo.2019.05.015

Rey J, Martínez J, Hidalgo MC, Mendoza R, Sandoval S (2021) Assessment of tailings ponds by a combination of electrical (ERT and IP) and hydrochemical techniques (Linares, southern Spain). Mine Water Environ. https://doi.org/10.1007/s10230-020-00709-3

Reynolds JM (2011) An introduction to applied and environmental geophysics, 2nd edn. Wiley-Blackwell, London

Rotta LHS, Alcântara E, Park E, Negri RG, Lin YN, Bernardo N, Mendes TSG, Filho CRS (2020) The 2019 Brumadinho tailings dam collapse: possible cause and impacts of the worst human and environmental disaster in Brazil. Int J Appl Earth Obs Geoinf 90:102119. https://doi.org/10.1016/j.jag.2020.102119

Schorscher HD, Osmond JK (1992) Origin and growth rates of pitchblende nodules at the Osamu Utsumi mine, Poços de Caldas, Brazil. J Geochem Explor 45:159–171. https://doi.org/10.1016/0375-6742(92)90124-Q

Schorscher HD, Shea ME (1992) The regional geology of the Poços de Caldas alkaline complex: mineralogy and geochemistry of selected nepheline syenites and phonolites. J Geochem Explor 45:25–51

Silva MP, Moreira CA, Borssatto K, Ilha LM, Santos SF (2018) Geophysical prospection in tin mineral occurrence associated to greisen in granite São Sepé (RS). Int Eng J 71(2):183–189. https://doi.org/10.1590/0370-44672017710098

Simate GS, Ndlovu S (2014) Acid mine drainage: challenges and opportunities. J Environ Chem Eng 2(3):1786–1803. https://doi.org/10.1016/j.jece.2014.07.021

Souza AM, Silveira CS, Pereira RM (2013) Contribuições dos metais provenientes das pilhas de rejeito da Mina Osamu Utsumi a drenagens do Complexo Alcalino de Poços de Caldas, Minas Gerais. Geochim Bras 27:63–76. https://doi.org/10.21715/gb.v27i1.337 (**in Portuguese**)

Spitzer K, Chouteau M (2003) A DC resistivity and IP borehole survey at the Casa Berardi gold mine in northwestern Quebec. Geophysics 68:453–463. https://doi.org/10.1190/1.1567221

Targa DA, Moreira CA, Camarero PL, Casagrande MFC, Alberti HLC (2019) Structural analysis and geophysical survey for hydrogeological diagnosis in uranium mine, Poços de Caldas (Brazil). SN Appl Sci 1:299. https://doi.org/10.1007/s42452-019-0309-7

Telford WM, Geldart LP, Sheriff RE (1990) Resistivity methods. In: Applied geophysics, 2nd edn. Cambridge Univ Press, Cambridge, pp 353–358. https://doi.org/10.1017/cbo9781139167932.012

Thompson F, Oliveira BC, Cordeiro MC, Mais BP, Rangel TP, Paz P, Freitas T, Lopes G, Silva BS, Cabral A, Soares M, Lacerda D, Vergilio CS, Lopes-Ferreira M, Silva CL, Thompson C, Resende CE (2020) Severe impacts of the Brumadinho dam failure (Minas Gerais, Brazil) on the water quality of the Paraopeba River. Sci Total Environ 705:135914. https://doi.org/10.1016/j.scitotenv.2019.135914

Urânio do Brasil S.A. (1988) Síntese dos trabalhos—Gerência da Mina de Caldas. Relatório Interno, Urânio do Brasil, Poços de Caldas, MG (**in Portuguese**)

Valeton I, Schumann A, Vinx R, Wieneke M (1997) Supergene alteration since the upper cretaceous on alkaline igneous and metasomatic rocks of the Poços de Caldas ring complex, Minas Gerais, Brazil. Appl Geochem 12:133–154. https://doi.org/10.1016/S0883-2927(96)00060-1

Veiga LHS, Koifman S, Melo VP, Sachet I, Amaral ECS (2003) Preliminary indoor radon risk assessment at the Poços de Caldas Plateau, MG-Brazil. J Environ Radioact 70:161–176. https://doi.org/10.1016/S0265-931X(03)00101-2

Vieira LB, Moreira CA, Côrtes RP, Luvizotto GL (2016) Geophysical modeling of the manganese deposit for Induced Polarization method in Itapira (Brazil). Geofís Int 55:107–117

Waber N (1992) The supergene thorium and rare-earth element deposit at Morro do Ferro, Poços de Caldas, Minas Gerais, Brazil. J Geochem Explor 45:113–157. https://doi.org/10.1016/0375-6742(92)90123-P

Waber N, Schorscher HD, Tj P (1992) Hydrothermal and supergene uranium mineralization at the Osamu Utsumi mine, Poços de Caldas, Minas Gerais, Brazil. J Geochem Explor 45:53–112. https://doi.org/10.1016/0375-6742(92)90122-O

Wardlaw S, Wagner R (1994) Development of waste rock sampling protocol using induced polarization. CANMET-MSL Div Nat Resour Can, Ottawa, LR, 777-071. Final Rept

Wiikmann LO (1998) Caracterização química e radiológica dos estéreis provenientes da mineração de urânio do Planalto de Poços de Caldas. MS Diss, Univ of São Paulo (**in Portuguese**)

Yang C, Lu G, Chen M, Xie Y, Guo C, Reinfelder J, Yi X, Wang H, Dang Z (2016) Spatial and temporal distributions of sulfur species in paddy soils affected by acid mine drainage in Dabaoshan sulfide mining area, South China. Geoderma 281:21–29. https://doi.org/10.1016/j.geoderma.2016.06.032

Yuval D, Oldenburg W (1996) DC resistivity and IP methods in acid mine drainage problems: results from the Copper Cliff mine tailings impoundments. J Appl Geophys 34:187–198. https://doi.org/10.1016/0926-9851(95)00020-8